Power and efficiency continuous modes in saturated GaN HEMT devices

Aleksander Bogusz, Zack Costello, Roberto Quaglia, James Bell, Jonathan Lees, Paul Tasker, Steve Cripps

Centre for High Frequency Engineering, Cardiff University, United Kingdom
e-mail: bogusza@cardiff.ac.uk

***Abstract*—This paper discusses, for the first time, the continuity of optimum load for power and efficiency in saturated GaN devices. Continuous modes are defined originally on the zero-grazing voltage assumption. In this paper we show that a continuous behaviour can also be observed in saturated devices without imposing any limitation on clipping. Simulations using a simplified knee-model for the device and source-load pull experimental characterization are critically analysed and compared to describe the discovered continuum.**

***Index Terms*—Gallium nitride, modelling, power amplifiers, contours.**

I. Introduction

Power amplifiers (PAs) are crucial components of high frequency transmitters since they deeply affect the transmitter performance in terms of output power, signal fidelity and energy efficiency [1]. PA designers often must deal with contrasting requirements leading to trade-offs. One typical example of this compromise is efficiency vs. bandwidth; the former improvable thanks to harmonic tuning that degrades the latter due to the resonant structures needed for harmonic control requiring a very careful approach to optimize the design [2]. A recent and important discovery in PA design has been continuous modes [3], which have enabled the combination of harmonic tuning and broadband operation. Originally introduced as an extension of class B for purely reactive second harmonic terminations, it has now been applied to many different PA classes and cases [4], [5], [6].

The basic assumption made in the construction of continuous modes is the zero-grazing condition for the voltage waveform, that limits the clipping of the current waveform and leads to the definition of the continuum itself. On the other hand, devices in saturated conditions exhibit stronger non-linear behaviour that require ad-hoc modelling [7], but that can be useful in several PA applications.

In this paper, the continuity of power and efficiency optimum impedances in GaN HEMT devices driven into saturation is explored, for the first time, using a simplified knee-model [8]. Source/Load-Pull characterization is then used to critically compare the results with experimental data.

II. Principle

For an ideal device with drain bias voltage V_{DD} and maximum current I_{MAX}, biased in class B with shorted harmonic terminations, the optimum load is $R_{\mathrm{OPT}} = 2V_{\mathrm{DD}}/I_{\mathrm{MAX}}$ for both maximum power and efficiency. This result assumes a half sinusoidal current waveform and no knee effect, and leads to an output power of $P_{\mathrm{MAX}} = 0.25V_{\mathrm{DD}}I_{\mathrm{MAX}}$ and efficiency $\eta_{\mathrm{MAX}} = \pi/4$ [3]. For the same drain current waveforms, the continuous modes are defined as the voltage waveforms whose minimums graze zero and that lead to the same P_{MAX} and η_{MAX}. Having defined a constant current waveform and a continuum of voltage waveforms, it is possible to derive the harmonic impedance continuum by dividing the voltage Fourier components by the current components. This leads to the well-known definition of the class B- class J continuum in terms of fundamental and second harmonic loads Z_1 and Z_2:

$$\begin{cases} Z_1 = R_{\mathrm{OPT}}\left(1 - j\beta\right) \\ Z_2 = j\frac{3\pi}{8}R_{\mathrm{OPT}}\beta \end{cases} \tag{1}$$

where β is a real free parameter with $|\beta| \leq 1$. This result has been widely adopted and can enable high-efficiency broadband design in linear power amplifiers.

However, when driving the device deeper into compression, some assumptions on the ideal device can no longer be sustained. For example, in devices with a smooth knee behaviour, such as GaN devices, the optimum loads for maximum power and efficiency are quite far apart, with the optimum for efficiency around twice the optimum for power [9], [8]. Moreover, while for linear operation it is enough to substitute the zero-grazing condition with a knee-grazing condition, in saturation this approximation does not make sense anymore, since the knee can be explored down to 0 V, or lower [8].

Since a simplified knee voltage model has been successfully adopted to predict power and efficiency optimum loads in GaN devices [8], the same model is used here to explore how the optimum fundamental loads for power and efficiency change when the second harmonic is not at $0\,\Omega$. This allows us to explore the continuity of power and efficiency terminations in saturation.

Given a baseline current $a(t)$, i.e., the current the drain would drive without knee effect, the real drain current can be written as:

$$i_{\mathrm{D}}(t) = a\left(t\right)\left[1 - \left(1 - v_{\mathrm{DS}}\left(t\right)\right)^{N}\right] \tag{2}$$

where v_{DS} is the drain-to-source voltage and N is an even integer, that ranges between 4 and 8 to model GaN devices.

This formulation creates a dependence between voltage and current. In [8], the higher harmonics are all assumed to be short-circuited and the resulting simplified voltage allows for a general analytical solution. Setting the second harmonic to an arbitrary reactance makes the analysis very complicated, so in this work the model is implemented in a simulator to study the continuum. In particular, an symbolically defined device component is used in Advance Design System (ADS)

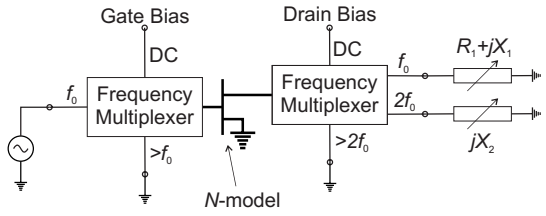

Fig. 1. Schematic of the simulation template used for determining the optimum loads for maximum power and efficiency with the N model.

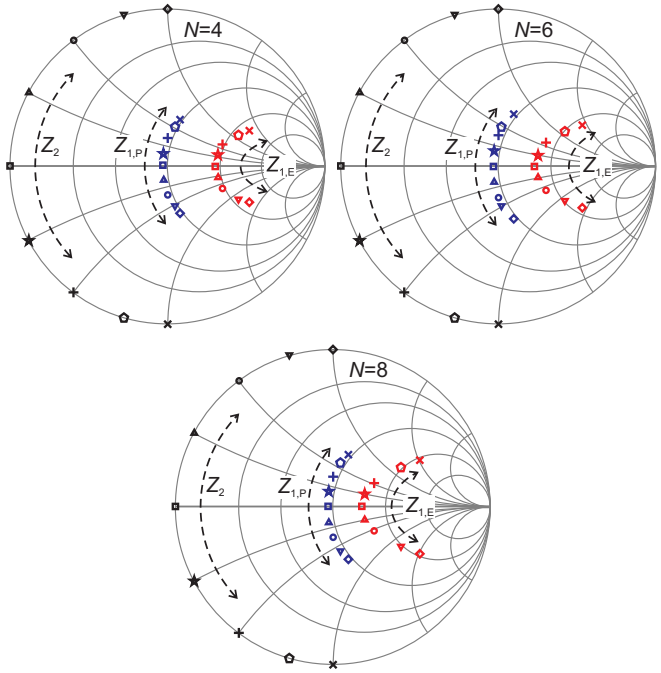

Fig. 2. Power and efficiency optimum fundamental loads (Z_{1P}, Z_{1E}) determined for different second harmonic terminations Z_2, for $N = 4, 6, 8$.

to implement (2) and simulate the simplified device in a load-pull template. In particular, the fundamental load is swept on a grid inside the Smith Chart, while the second harmonic load is swept on the border of the Smith Chart. Source harmonic terminations are all short-circuited. Fig. 1 shows a schematic of the simulation setup.

Fig. 2 shows the position of the optimum fundamental impedance for maximum power and efficiency (Z_{1P}, Z_{1E}) at different second harmonic loads Z_2 for $N = 4$, $N = 6$, and $N = 8$. The Smith Chart is normalized at R_{OPT}. The first important result is that a continuum can be observed, and that it has a similar trend compared to the original continuous modes. In fact, for increasing second harmonic reactance, the optimum fundamental loads have an increasing reactance with opposite sign [3]. The optimum for output power maintains a relatively constant real part, while the optimum for efficiency has a larger distortion and tends to increase for larger $|Z_2|$. The second important thing to notice is that N has quite a visible impact on the position of the optimum impedance, especially for efficiency. For this emulation, this means that the knee profile is key to shaping the optimum efficiency.

III. Experimental Results

To verify that the continuum can be observed experimentally, source/load pull characterization is adopted to recreate the environment shown in Fig. 1. In particular, using the facilities at Cardiff University, the setup represented in Fig. 3 has been used. It consists of an active source/load pull system with 3 harmonics. A comb-generator is used as a phase

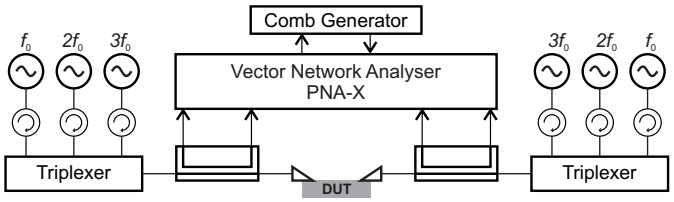

Fig. 3. Diagram of the measurement setup used for characterization.

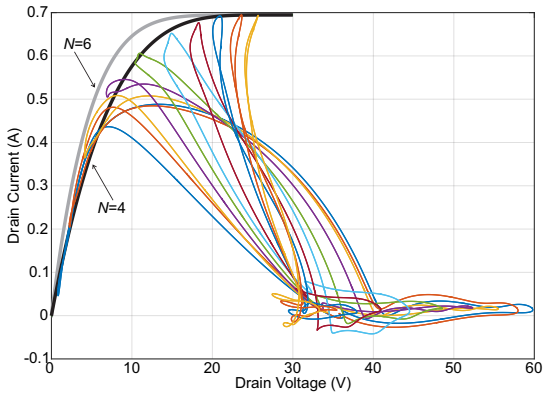

Fig. 4. Measured fan diagram at 900 MHz of the 6x130 μm device. N-model approximation with N=4 and N=6.

reference to reconstruct the waveforms at calibration plane by re-aligning the harmonic components measured by the system. Although not necessary for the determination of the optimum loads, the waveforms have been used to draw the so-called fan diagram [10]; used to fit the $N-$model. Fig. 4 shows the fan-diagram of a 6x130 μm device based on GaN 250nm HEMT technology, with N=4 providing a good fit. The drain bias voltage is V_{DD}=28 V; the quiescent drain current is in very deep class AB (13 mA); and from Fig. 4 a maximum current I_{MAX}=0.695 A can be observed. Another device has also been measured, an 8x80 μm device based on the same technology. Its fan diagram, not shown here to save space, it also fits well with N=4. For this device, the drain bias voltage is V_{DD}=28 V; the quiescent drain current is 11 mA; and I_{MAX}=0.58 A. A first set of measurements was used to identify the optimum load for output power and efficiency with shorted harmonics, with a drive power level that saturates the device. The optimum loads are also chosen to estimate the output capacitance in order to deembed the reference plane – placing it at the

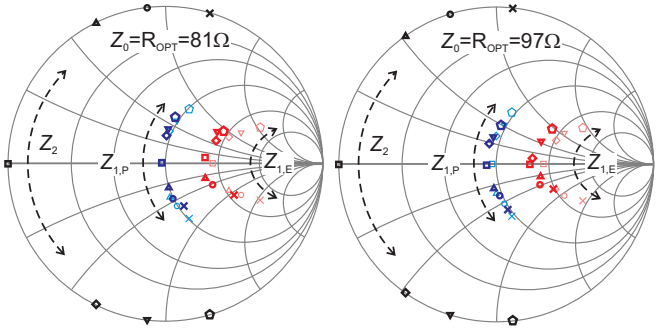

Fig. 5. Power and efficiency optimum fundamental loads (Z_{1P}, Z_{1E}) determined for different second harmonic terminations Z_2. 6x130 μm device (left), 8x80 μm device (right). Measured: Dark coloured symbols; Simulated with N=4: Light coloured symbols.

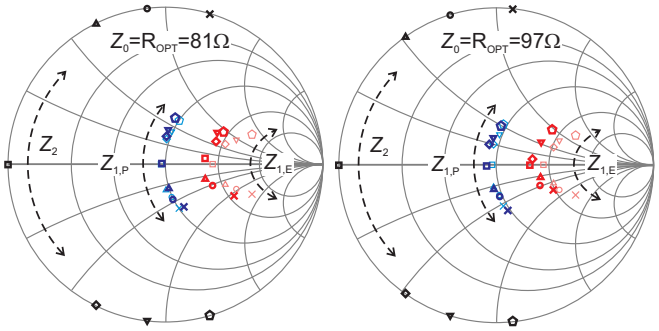

Fig. 6. Power and efficiency optimum fundamental loads (Z_{1P}, Z_{1E}) determined for different second harmonic terminations Z_2. 6x130 μm device (left), 8x80 μm device (right). Measured: Dark coloured symbols; Simulated with N=4 and scaling of imaginary impedance: Light coloured symbols.

intrinsic current generator – for an easier comparison with the N-model results. The search for optimum fundamental loads was then repeated at different Z_2 values. Fig. 5 shows the resulting optimum loads on both the devices. The Smith Charts refer to the intrinsic generator plane and are normalized to $R_{\rm opt} = 2V_{\rm DD}/I_{\rm MAX}$, with the $I_{\rm MAX}$ determined from the fan-diagrams. On initial inspection, the optimum power impedance continuum is clearly present, and agrees well with the predictions for both devices. The main difference with the simulations is the extension of the imaginary components of the impedance continuum. An explanation for this can be found in the device drain current baseline that is not an ideal truncated sinewave. In fact, for both devices, the ratio between second and fundamental Fourier components of drain current for negligible knee interaction is approximately $\simeq 0.31$, while it is $\simeq 0.42$ in the ideal case. This means that the imaginary part of the second harmonic voltage in the real device is, at the same second harmonic impedance, lower than expected, leading to a lower fundamental imaginary part needed to compensate.

Fig. 6 shows the same measured optimum loads, but this time compared with the simulated ones whose imaginary part of the impedance has been scaled by a factor $0.31/0.42$. This is a very rough approximation, since the scaling of the second harmonic current in the baseline function does not guarantee the same scaling in the total current once it has been through the non-linear knee-function. Nevertheless, it has yielded a rather accurate adjustment of the simulated optimum impedances for output power.

Conversely, the optimum efficiency impedances are predicted less accurately, however, a continuum can still be clearly observed. This is also true when applying scaling to the imaginary impedance components. This can be attributed to a stronger interaction with the knee in this higher impedance region that decreases the accuracy of the linear scaling applied.

IV. Conclusion

The continuum of maximum power and maximum efficiency fundamental loads for a saturated GaN device has been predicted, using a simplified knee-model, and verified through measurements for the first time. The proposed model shows good accuracy when predicting the optimum power loads, with the accuracy further improved by a linear scaling deducible from the drain current Fourier components. The trend of the optimum efficiency loads is also indicated by simulations, while the prediction of the exact loads is less accurate and requires further analysis.

References

[1] F. Raab, P. Asbeck, S. Cripps, P. Kennington, Z. Popovic, N. Pothecary, J. Sevic, and N. Sokal, "Power amplifiers and transmitters for RF and microwave," *IEEE Trans. Microw. Theory Techn.*, vol. 50, no. 3, pp. 814–826, Mar 2002.

[2] P. Colantonio, F. Giannini, R. Giofrè, and L. Piazzon, "Simultaneous dual-band high efficiency harmonic tuned power amplifier in GaN technology," in *Microwave Integrated Circuit Conference, 2007. EuMIC 2007. European*, 2007, pp. 127–130.

[3] S. Cripps, P. Tasker, A. Clarke, J. Lees, and J. Benedikt, "On the Continuity of High Efficiency Modes in Linear RF Power Amplifiers," *IEEE Microw. Wireless Compon. Lett.*, vol. 19, no. 10, pp. 665 – 667, Oct. 2009.

[4] T. Canning, P. J. Tasker, and S. C. Cripps, "Continuous mode power amplifier design using harmonic clipping contours: Theory and practice," *IEEE Trans. Microw. Theory Techn.*, vol. 62, no. 1, pp. 100–110, Jan. 2014.

[5] B. M. Merrick, J. B. King, and T. J. Brazil, "The continuous harmonic-tuned power amplifier," *IEEE Microw. Wireless Compon. Lett.*, vol. 25, no. 11, pp. 736–738, Nov. 2015.

[6] R. Quaglia, J. J. Bell, and S. Cripps, "New general formulation and experimental verification of harmonic clipping contours in high-frequency power devices," *IEEE Trans. Microw. Theory Techn.*, vol. 65, no. 10, pp. 3903–3909, Oct. 2017.

[7] A. Raffo, F. Scappaviva, and G. Vannini, "A new approach to microwave power amplifier design based on the experimental characterization of the intrinsic electron-device load line," *IEEE Trans. Microw. Theory Techn.*, vol. 57, no. 7, pp. 1743–1752, July 2009.

[8] R. Quaglia, D. J. Shepphard, and S. Cripps, "A reappraisal of optimum output matching conditions in microwave power transistors," *IEEE Trans. Microw. Theory Techn.*, vol. 65, no. 3, pp. 838–845, Mar. 2017.

[9] J. Pedro, L. Nunes, and P. Cabral, "A Simple Method to Estimate the Output Power and Efficiency Load-Pull Contours of Class-B Power Amplifiers," *IEEE Trans. Microw. Theory Techn.*, vol. 63, no. 4, pp. 1239–1249, Apr. 2015.

[10] C. Roff, J. Benedikt, P. J. Tasker, D. J. Wallis, K. P. Hilton, J. O. Maclean, D. G. Hayes, M. J. Uren, and T. Martin, "Analysis of DC–RF Dispersion in AlGaN/GaN HFETs Using RF Waveform Engineering," *IEEE Trans. Electron Devices*, vol. 56, no. 1, pp. 13–19, Jan. 2009.